Proceedings 10th NUMGE 2023
10th European Conference on Numerical Methods in Geotechnical Engineering
Zdravkovic L, Kontoe S, Taborda DMG, Tsiampousi A (eds)

https://doi.org/10.53243/NUMGE2023-24

Numerical evaluation on the performance of deep excavation with the strut-free retaining system in clays

A. S. Abdi[1], C. Y. Ou[2]

[1,2]*Department of Civil and Construction Engineering, National Taiwan University of Science and Technology, Taipei, Taiwan.*

ABSTRACT: This paper aims to evaluate the performance of a novel strut-free excavation system in clays using three-dimensional finite element analyses. This system typically consists of the diaphragm wall, buttress wall, cross wall, and capping slab. The results revealed that the installation of the buttress wall would provide additional frictional and bearing resistance, which could enhance the overall stability. On the other hand, implementing the cross wall would cause the failure surface to extend far behind and below the diaphragm wall, resulting in a significant increase in the factor of safety. In addition, a new schematic of a strut-free excavation system was proposed by combining buttress wall and ground improvement, which can be used as an alternative and innovative solution for deep excavation design. Based on these findings, a new simplified method was proposed to assess the factor of safety for a strut-free excavation system with a buttress wall, cross wall, and ground improvement.

Keywords: Buttress wall; Cross wall; Deep excavation; Factor of safety; Ground improvement

1 INTRODUCTION

A novel strut-free excavation system is specifically adapted to optimize working space, shorten the construction period, and effectively reduce excessive wall displacement, which has been verified through comprehensive studies and case histories (Lim et al. 2020; Yeh et al. 2022). This system generally consists of the installation of diaphragm walls (DW), buttress walls (BW), cross walls (CW), and capping slabs (CS). A series of three-dimensional finite element methods (3D FEM) was performed to evaluate the performance of the strut-free excavation system to the deformation and stability analysis. Additionally, new schematics of strut-free excavation system by combining BW and ground improvement (GI) was also introduced as an alternative and innovative solution. Finally, a new simplified method was proposed to assess the factor of safety for a strut-free excavation system, which was verified by the 3D FEM results.

2 NUMERICAL MODELING

The Plaxis 3D FEM was used to conduct the schematic behavior of BW, CW, and GI. All structural components were modeled as plate elements, where Young's modulus was estimated by using $E = 4700\sqrt{f_c'}$ (f_c' = 27.5 MPa) (ACI 1995). The slippage behavior between the structure and soil was modeled by the interface element, which is controlled by the frictional resistance ratio of wall adhesion and undrained shear strength ($\alpha = c_w/s_u$).

Two possible BW shapes were selected, such as the R-BW (rectangular shape) and T-BW (similar to the capital letter T). Four different models were considered for the hypothetical cases, as illustrated in Figure 1. The BW length, BW flange, BW depth, CW depth, GI depth, BW spacing, and CW spacing were denoted as L_{bw}, F_{bw}, D_{bw}, D_{cw}, D_{GI}, s_{bw}, and s_{cw}, respectively. The thickness of DW, BW, and CW was assumed to be 0.7 m, while the CS thickness was 0.4 m. The BW, CW, and GI were implemented directly after installing the DW. The soil is excavated uniformly (3 m intervals) until it reaches the final excavation level (H_e = 12 m). The BW part was maintained during the excavation, while the CS was installed after finishing the first excavation stage. Figure 2 shows the finite element mesh used in the analysis.

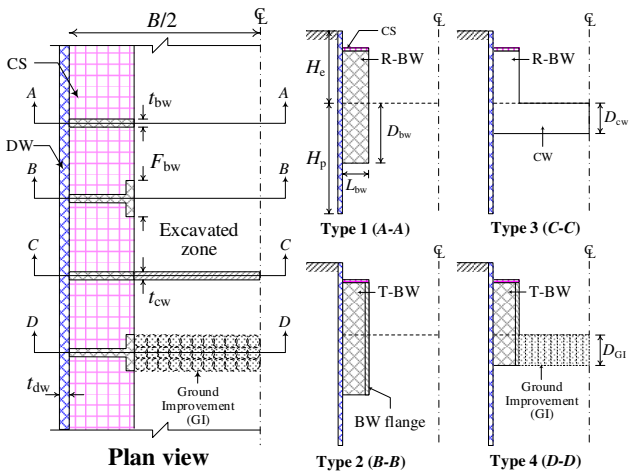

Figure 1. Different types of strut-free excavation systems.

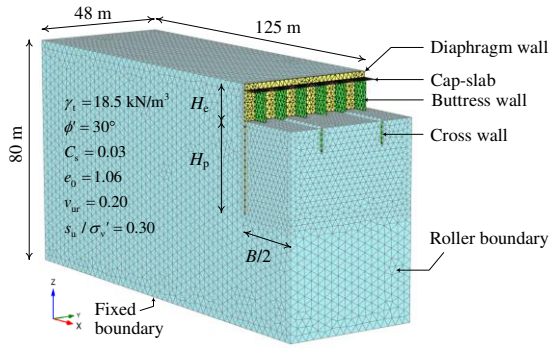

Figure 2. Finite element mesh used in the analysis.

The stability analysis with the strength reduction method was performed to assess the factor of safety (FS_{fem}) at the final stage. Because the stress-dependent stiffness and hardening effect of soil were excluded in the strength reduction method, the total stress Mohr-Coulomb soil model is appropriate to simulate the undrained behavior of the clay and soil strength characteristic near failure (Abdi and Ou 2022; Goh et al. 2019). A normally consolidated clay was considered for the analysis, where the soil parameters were adopted based on the typical Taipei clay (Lim and Ou, 2017), as detailed in Figure 2. The elastic Young's modulus unloading/reloading (E_{ur}) was determined by using Equation (1) (Lim et al, 2010). The E_{ur} value was further converted to be undrained Young's modulus (E_u) by using Equation (2).

$$E_{ur} = \frac{3(1+e_0)p'(1-2\nu_{ur})}{C_s/\ln(10)} \quad (1)$$

$$G_{ur} = \frac{E_{ur}}{2(1+\nu_{ur})} = \frac{E_u}{2(1+\nu_u)} = G_u \quad (2)$$

where e_0 is the initial void ratio, p' is the mean effective stress, ν_{ur} and ν_u are the unloading/reloading and undrained poisson's ratio, respectively. Assuming that ν_{ur} = 0.2 and ν_u = 0.5, then $E_u = 1.25E_{ur}$.

For the GI properties, the unconfined compressive strength (q_u) ranged from 1 to 3 MPa (Ou et al. 1996). The tensile strength and Young's modulus of GI can be assumed as $\sigma_t = 0.29q_u$ and $E_{50} = 250q_u$, respectively, following the typical treated soil of Taipei clay (Chen 2003; Fang et al. 1997; Liao 2002). Poisson's ratio (ν) of GI is 0.30 (Shibazaki and Ohta, 1982). Moreover, the GI was simulated by using non-porous soil model.

3 PERFORMANCE OF STRUT-FREE EXCAVATION SYSTEM

3.1 Deformation and internal force characteristic of the strut-free retaining system

Figure 3(a) shows the computed wall displacement at the final stage for H_p/H_e = 2.5 and B = 30 m (Type 1: L_{bw}/H_e = 1.0, s_{bw} = 6 m; Type 2: L_{bw}/H_e = 0.75, F_{bw} = 3 m, s_{bw} = 6 m; Type 3: D_{cw}/H_p = 0.25, s_{cw} = 12 m; Type 4: L_{bw}/H_e = 0.5, F_{bw} = 3 m, D_{GI}/H_p = 0.25, s_{bw} = 12 m). The results showed that the computed wall displacement for types 1 and 2 exhibit the cantilever shape caused by the long embedded wall that is fixed below the excavation level. Besides, R-BW is rather than T-BW in restraining the wall displacement for the same amount of concrete material. This is due to the frictional resistance that fully mobilizes for R-BW, while the BW flange (F_{bw}) in T-BW would decrease the frictional resistance on the BW length. Furthermore, combining the BW and CW (type 3) or implementing T-BW along with GI (type 4: q_u = 1–3 MPa) could significantly reduce the wall displacement along the depth.

The maximum bending moment of DW (M_{max}) for different excavation stages was also evaluated, as shown in Figure 3(b). It is found that implementing CW (type 3) would produce a higher M_{max} value as compared to that without CW (types 1 and 2). Interestingly, the M_{max} value for type 4 is relatively lower than that of type 3, while these two types yielded similar wall displacement results (see Figure 3(a)). This implies that type 4 has a promising prospect as an effective measure to control the movement and bending moment of DW.

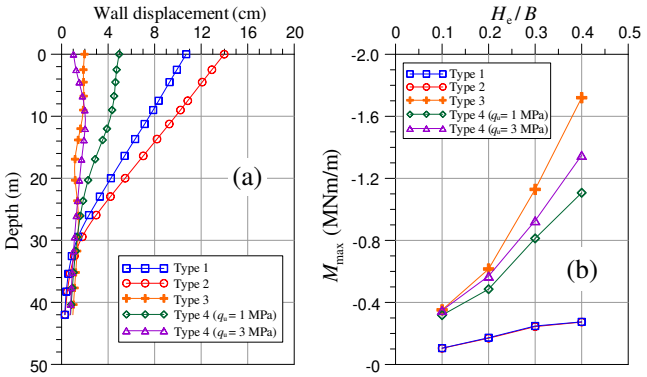

Figure 3. Finite element results: (a) computed wall displacement at the final stage; (b) M_{max} varied by excavation depths.

The axial force of BW and CW at the final stage was further evaluated, as shown in Figure 4(a). The results for D_{cw} = 7.5 m showed that higher axial force acted below the excavation level. The highest axial force (N_{max}) was located at the lowest level of the DW-CW and BW-CW connection. Besides, the N_{max} value was increased significantly for a shorter D_{cw} (D_{cw} = 2.5 m). These findings should be highlighted when designing strut-free excavation system with CW.

Figure 4(b) shows the schematics behavior of the retaining system for type 3. It is found that the relative shear stress (τ_{rel}) for q_u = 3 MPa was lower than q_u = 1 MPa, indicating that the GI tends to shear failure for lower q_u. As a result, the magnitude of N_{max} on BW was reduced for lower q_u. Nevertheless, the N_{max} value for type 4 is much lower than that of type 3, implying that this proposed model could be recommended as an alternative solution.

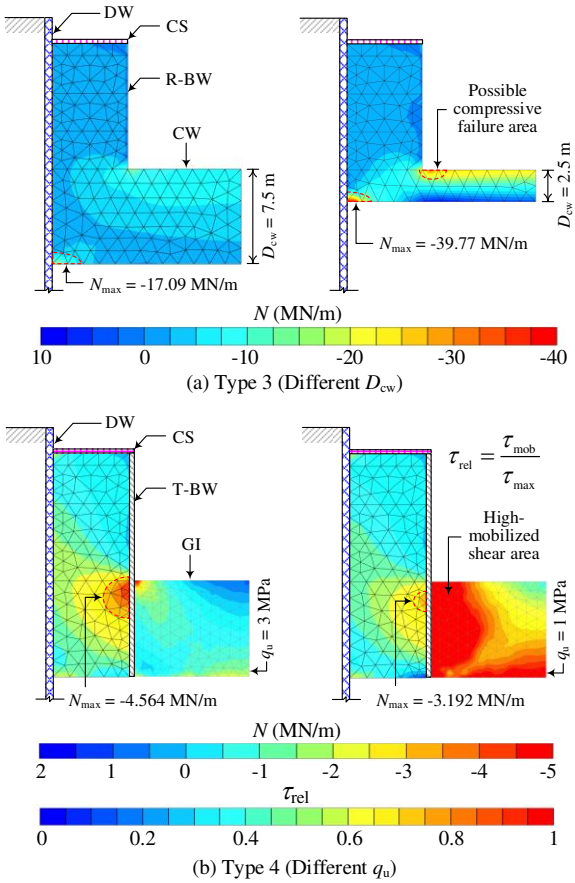

Figure 4. Performance of retaining system at the final stage: (a) Type 3 (different D_{cw}); (b) Type 4 (different q_u).

3.2 Stability mechanism of BW, CW, & GI

Figure 5(a) and (b) show the FS_{fem} values varied by α value and H_p/H_e ratio. It is found that the FS_{fem} values from type 1 were slightly higher than type 2 for a rigid BW surface ($\alpha_{bw} = 1.0$). However, for a very smooth BW surface ($\alpha_{bw} = 0.1$), the FS_{fem} values from type 1 are close to that without BW, whereas the results from type 2 are relatively higher. The FS_{fem} values were significantly increased for type 3, where reducing α_{cw} values could decrease the FS_{fem}. This implies that the frictional resistance on BW and CW interface could contribute to the stability resistance. For type 4, the FS_{fem} values were enhanced as the q_u values increased.

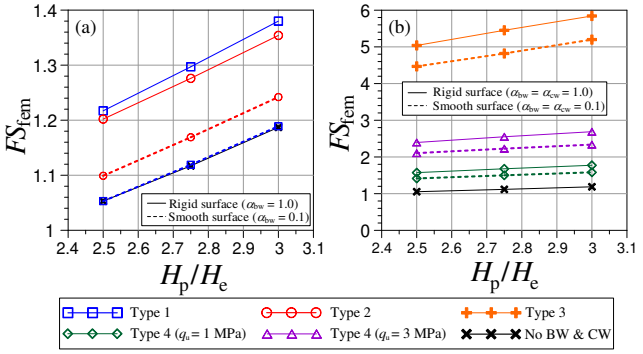

Figure 5. Variation of the factor of safety for different α and H_p/H_e (B = 30 m): (a) Type 1 and 2; (b) Type 3 and 4.

In order to clarify the above findings, the typical failure surface of the strut-free system with different types was introduced by observing the ground movement vector at ultimate conditions. As shown in Figure 6(a), (b), and (d), the overturning failure occurred when no CW was considered. Meanwhile, the typical basal heave failure was found for the case with CW, where the soil behind the wall was moving downward, passing through below the wall toe, causing the large upward movement inside the excavation (Figure 6c). Under such a case, an integrated retaining system was established, resulting in a higher stability resistance than that of without CW.

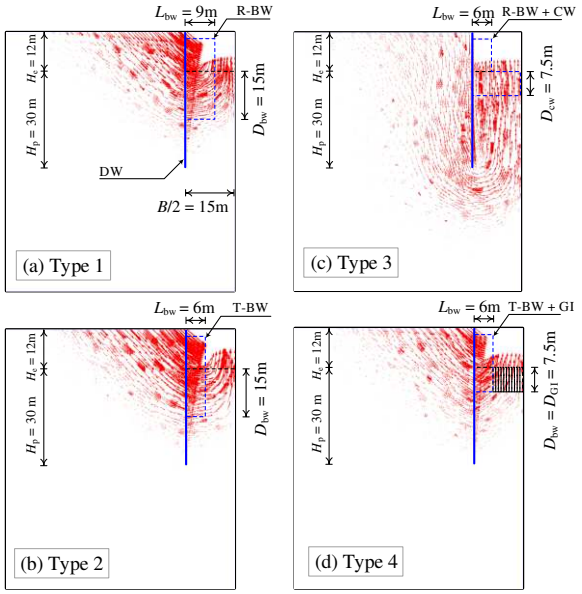

Figure 6. Typical failure surface of excavation with strut-free system: (a) Type 1; (b) Type 2; (c) Type 3; (d) Type 4.

3.3 Different BW, CW, & GI dimension

As shown in Figure 7, increasing the BW length or shortening the BW spacing could increase the overall stability resistance, resulting in a higher FS_{fem}. Besides, the FS_{fem} for types 1 and 2 is typically similar for the same amount of BW material. However, a wider excavation would reduce the overall stability resistance, causing a non-linear increase of FS_{fem} when enlarging the BW length towards the middle of the excavation. In such a case, the BW length should be sufficiently long to enhance the overall stability resistance effectively.

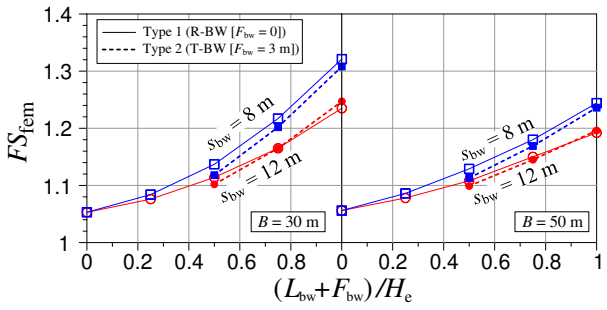

Figure 7. Variation of factor of safety for different BW dimensions for types 1 and 2 (H_p/H_e = 2.5; B = 30 - 50 m).

Figure 8 shows the FS_{fem} values for different CW and GI dimensions. Similar to types 1 and 2, enlarging the CW and GI dimension for types 3 and 4 could also enhance the overall stability resistance. Additionally, wider excavation could slightly reduce the stability resistance. Although type 3 generally performed the best in enhancing the stability resistance, type 4 could still satisfy the factor of safety ($FS_{fem} \geq 1.20$).

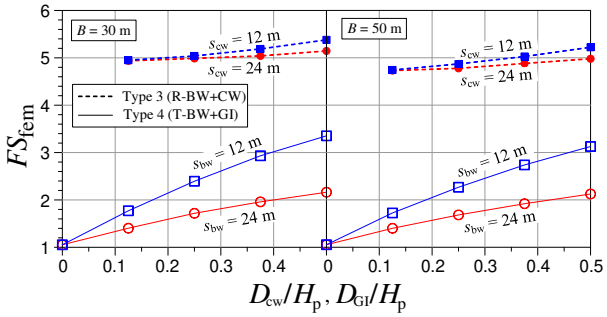

Figure 8. Variation of the factor of safety for different CW and GI dimensions varied by Type 3 and Type 4 (q_u = 3 MPa) (H_p/H_e = 2.5; B = 30 - 50 m).

4 PROPOSED SIMPLIFIED METHOD

4.1 Strut-free excavation system with BW & GI

According to Figure 6, the overturning failure occurred for the case without CW, so the factor of safety can be defined as the ratio of the moment resisting (M_r) to the moment driving (M_d). Besides, the wall will rotate near the wall toe at failure condition, as indicated in Figure 6. According to Madabushi and Chandrasekaran (2005), the wall will rotate at pivot point (z) where the resistance to rotation is minimum, which can be achieved by minimizing the moment ratio ($M = M_r/M_d$). Assuming that the location of z occurred below the final excavation and then conducted the force equilibrium analysis to obtain z. The lateral earth pressure acting on the wall ($\sigma_{ha,hp}$) can be expressed as (Padfield and Mair, 1984):

$$\sigma_{ha,hp} = \sigma_v K_{a,p} \mp 2s_u\sqrt{K_{a,p}(1+\alpha)} \quad (3)$$

where σ_v is the overburden pressure, K_a and K_p are the coefficient of active and passive earth pressure, respectively ($K_a = K_p = 1$ for $\phi = 0$), and α is the frictional resistance ratio of wall interface ($\alpha = c_w/s_u$).

Figure 9(a) plots the estimation of pivot location (z/H_p) for different H_p/H_e. It is found that the least minimum moment ratio was changed as the H_p/H_e ratio increased. The location of the pivot point was further adopted to estimate the lateral earth pressure along the depth for H_p/H_e = 3.0. The close agreement between the FEM results and simplified approach was obtained for the earth pressure distribution (see Figure 9(b)). Hence, this method can be reasonably adopted for estimating the FS value without the CW system.

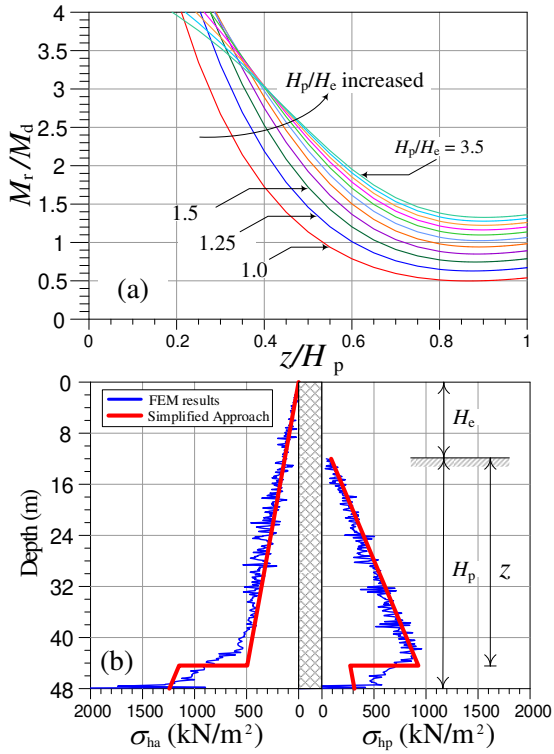

Figure 9. Schematics of excavation without supporting system: (a) minimization moment ratio to obtain the location of pivot point; (b) earth pressure distribution.

In order to account for the existence of BW and GI, the formula was modified by assuming that the additional moment resistance (i.e., additional frictional and bearing resistance on BW length and flange) acted equivalently along the width section of DW, as shown in Figure 10. In addition, the self-weight of BW and CS could also affect to the factor of safety. Thus, the proposed simplified method for estimating the factor of safety of strut-free excavation system with BW system (FS_{bw}^{sf}) can be expressed as:

$$FS_{bw}^{sf} = \frac{\sum M_r}{\sum M_d} = \frac{P_p L_p + P_{bw,f} L_f + P_{bw,b} L_b}{P_a L_a + M_{cs} + M_{bw}} \quad (4)$$

$$P_{bw,f} = s_{u,bw}\eta_f\left(\frac{2\alpha_{bw} L_{bw} D_{bw}}{s_{bw}}\right) \quad (5)$$

$$P_{bw,b} = \sigma_{hp}\eta_b\left(\frac{F_{bw} D_{bw}}{s_{bw}}\right) \quad (6)$$

$$M_{cs} = \sum \frac{P_{cs} L_{cs}}{2} = \frac{(n)\gamma_{cs} t_{cs} L_{cs}^2}{2} \quad (7)$$

$$M_{bw} = \sum M_L + \sum M_F = \frac{\gamma_{bw} t_{bw} L_{bw} H_B (F_{bw} + 0.5 L_{bw})}{s_{bw}} \quad (8)$$

where P_a and P_p are the resultant of the active and passive earth pressure; $P_{bw,f}$ and $P_{bw,b}$ are the equivalent force from BW friction and bearing resistance; L_a, L_p, L_f, L_b are the length from the pivot point to the point of action; γ_{bw} and γ_{cs} are the unit weight of BW and CS, respectively; and $s_{u,bw}$ is the variation of undrained shear strength along the BW penetration depth.

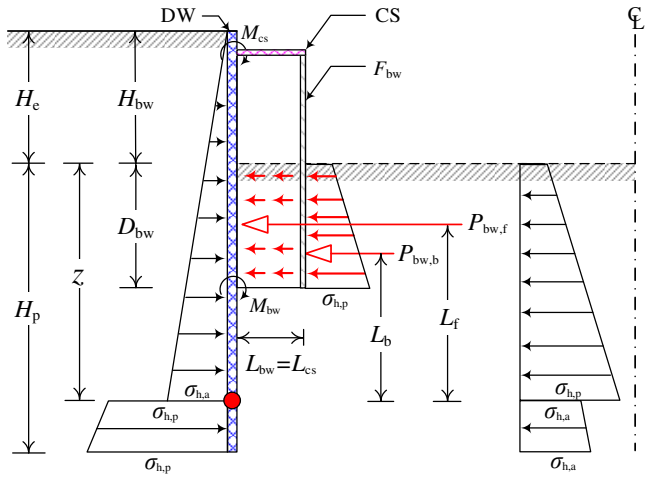

Figure 10. Proposed modified earth equilibrium method for excavation stability with BW, CS, and GI.

Because the BW stability resistance (types 1 and 2) was affected by excavation width, modification factor of BW frictional (η_f) and bearing resistance (η_b) associated with L_{bw}/B was proposed by performing random cases for different B, L_{bw}, s_{bw}, and F_{bw}. As shown in Figure 11(a), the distribution points tend to increase linearly and exponentially, which can be defined as:

$$\eta_f = 1.507\left(\frac{L_{bw}}{B}\right) + 0.287 \tag{9}$$

$$\eta_b = 0.0927e^{5.6635(L_{bw}/B)} \tag{10}$$

Although the additional bearing resistance was mainly controlled by GI for type 4, the frictional resistance on BW length could still contribute to the overall stability resistance at the certain L_{bw}/B ratio (Figure 11(b)). Thus, the modification factors (η_f and η_b) for type 4 can be expressed as:

$$\eta_f = 3.04\left(\frac{L_{bw}}{B}\right) - 0.064 \tag{11}$$

$$\eta_b = 0.576\left(\frac{L_{bw}}{B}\right) + 0.645 \tag{12}$$

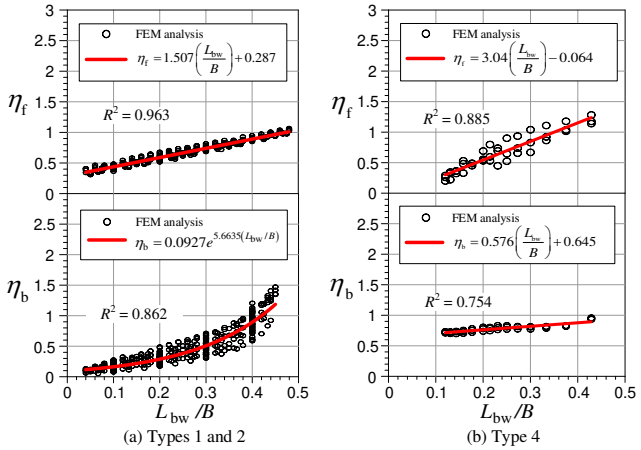

Figure 11. The modification factor for BW frictional and bearing resistance: (a) types 1 and 2; (b) type 4

4.2 *Strut-free excavation system with CW*

According to Figure 6(c), the failure mechanism of the strut-free excavation system with CW is the basal heave failure rather than the overturning failure. Hence, the proposed simplified method was derived on the basis of the original Terzaghi's bearing capacity theory (Equation (13)). As shown in Figure 12, the original Terzaghi's failure surface was extended below the wall toe to define the proposed modified Terzaghi's failure surface. Under such conditions, the modified formula can be expressed by Equation (14). Furthermore, the overall CW frictional resistance were assumed to be acted equivalently along the width section of DW. Finally, the modified Terzaghi's method with considering CW system can be defined by Equation 15.

$$FS_T = \frac{5.7s_{u,b}B'}{\gamma H_e B' - s_{u,a}H_e} \tag{13}$$

$$FS_{mT} = \frac{5.7s_{u,3}B' + s_{u,2}H_p(1+\alpha_{dw})}{\gamma H_e B' - s_{u,1}H_e} \tag{14}$$

$$FS_{cw}^{sf} = \frac{5.7s_{u,3}B' + s_{u,2}H_p(1+\alpha_{dw}) + s_{u,cw}\beta_{cw}}{\gamma H_e B' - s_{u,1}H_e} \tag{15}$$

$$\beta_{cw} = \frac{2\alpha_{cw}D_{cw}0.5B}{s_{cw}} = \frac{\alpha_{cw}D_{cw}B}{s_{cw}} \tag{16}$$

where γ is the soil unit weight; $B' = B\sqrt{2}$ is the radius of failure surface; $s_{u,a}$, $s_{u,b}$, $s_{u,1}$, $s_{u,2}$, $s_{u,3}$, $s_{u,cw}$ are the average undrained shear strength at the certain depth (see Figure 12); α_{cw} is the frictional resistance ratio of CW interface.

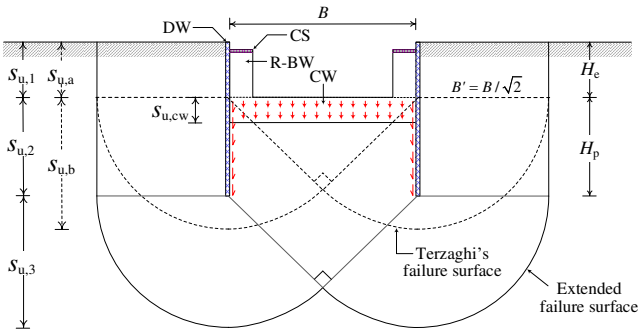

Figure 12. Proposed modified Terzaghi's method for excavation stability with CW.

4.3 *Results validation*

A total of 876 cases were conducted, which were varied by different properties of BW, CW, GI, and excavation geometries. As shown in Figure 13, the close agreements were obtained between the 3D FEM results and the proposed simplified method, where the data points are within ± 10% of the 1:1 line. This confirms that the simplified method is reasonably accurate and could be reasonably adopted in assessing the factor of safety for excavation stability with a strut-free system.

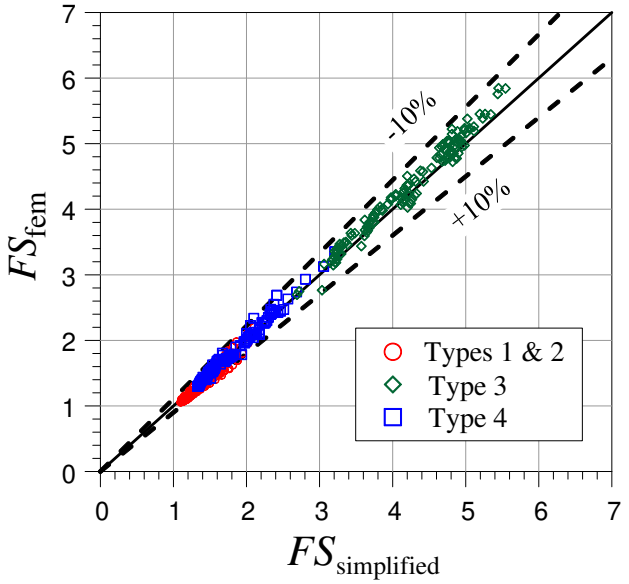

Figure 13. Comprehensive comparison of the factor of safety between the 3D FEM results and proposed simplified method.

5 CONCLUSIONS

This paper presents the numerical evaluation of the performance of the strut-free excavation system in clays. The results concluded that the stability resistance of a strut-free excavation system with a buttress wall was mainly governed by the frictional and bearing resistance that acted along the buttress wall length and flange, respectively. On the other hand, implementing the cross wall would establish an integrated retaining system, which could significantly increase the factor of safety.

A new schematic of the strut-free system was introduced by combining the buttress wall and ground improvement. This model performs well in restraining wall displacement and resisting overturning failure. Besides, the internal force of wall for this model is lesser than the cross wall system. Hence, this proposed model could be recommended as an alternative and innovative solution for excavation design.

A new simplified method was proposed to calculate the factor of safety for a strut-free excavation system with the cap-slab, buttress wall, cross wall, and ground improvement. The results concluded that the proposed simplified method could be reasonably adopted to assess the factor of safety, which was validated by the 3D FEM results through comprehensive comparisons.

6 ACKNOWLEDGEMENTS

The authors acknowledge the support provided by the Ministry of Science and Technology in Taiwan [grant number MOST 109-2221-E-011-015-MY3].

7 REFERENCES

Abdi, A. S., and Ou, C. Y. (2022). “A Study of the Failure Mechanism of Braced Excavations Using 3D Finite-Element Analysis.” *International Journal of Geomechanics*, 22(7), 1–14.

American Concrete Institute (1995). “Building Code Requirements for Structural Concrete.” *ACI 318R*, Farmington Hills, MI.

Chen, C. . (2003). “A study on the anisotropic strength of composite soil specimen using true triaxial testing.” National Taiwan University of Science and Technology.

Fang, Y. ., Liao, J. ., and Lin, T. K. (1997). “Mechanical properties of jet grouted soilcrete.” *Quarterly Journal of Engineering Geology*, 27, 257–265.

Goh, A. T. C., Zhang, W. G., and Wong, K. S. (2019). “Deterministic and reliability analysis of basal heave stability for excavation in spatial variable soils.” *Computers and Geotechnics*, Elsevier, 108, 152–160.

Liao, J. W. (2002). “Laboratory shear strength testing of composite soil specimen and its anisotropic characteristic.” National Taiwan Universtiy of Science and technology.

Lim, A., Ou, C. Y., and Hsieh, P. G. (2010). “Evaluation of clay constitutive models for analysis of deep excavation under undrained conditions.” *Journal of GeoEngineering*, 5(1), 9–20.

Lim, A., and Ou, C. Y. (2017). “Stress paths in deep excavations under undrained conditions and its influence on deformation analysis.” *Tunnelling and Underground Space Technology*, Elsevier Ltd, 63, 118–132.

Lim, A., Ou, C. Y., and Hsieh, P. G. (2020). “A novel strut-free retaining wall system for deep excavation in soft clay: numerical study.” *Acta Geotechnica*, Springer Berlin Heidelberg, 15(6), 1557–1576.

Madabhushi, S. P. G., and Chandrasekaran, V. S. (2005). “Rotation of Cantilever Sheet Pile Walls.” *Journal of Geotechnical and Geoenvironmental Engineering*, 131(2), 202–212.

Ou, C. Y., Wu, T. S., and Hsieh, H. S. (1996). “Analysis of Deep Excavation with Column Type of Ground Improvement in Soft Clay.” *Journal of Geotechnical Engineering*, 122(9), 709–716.

Padfield, C. J., and Mair, R. J. (1984). *Design of retaining walls embedded in stiff clays*. CIRIA Report No. 104, England.

Shibazaki, M. and Ohta, S. (1982). “A unique underpinning of soil solidfication utilizing super-high pressure liquid jet.” Proceedings, Conference on Grouting on Geotechnical Engineering, ASCE, New Orleans, 680-693.

Yeh, T., Ou, C.-Y., and Lim, A. (2022). “A case study of strut-free excavation retaining system.” *Acta Geotechnica*, Springer Berlin Heidelberg, 4.